New Journal of Physics
The open–access journal for physics

Simulation study of magnetic holes at the Earth's collisionless bow shock

B Eliasson[1] **and P K Shukla**
Institut für Theoretische Physik IV, Fakultät für Physik und Astronomie, Ruhr-Universität Bochum, D-44780 Bochum, Germany
and
Department of Physics, Umeå University, SE-90187 Umeå, Sweden
E-mail: bengt@tp4.rub.de

New Journal of Physics **9** (2007) 168
Received 25 April 2007
Published 21 June 2007
Online at http://www.njp.org/
doi:10.1088/1367-2630/9/6/168

Abstract. Recent observations by the Cluster and Double Star spacecraft at the Earth's bow shock have revealed localized magnetic field and density holes in the solar wind plasma. These structures are characterized by a local depletion of the magnetic field and the plasma density, and by a strong increase of the plasma temperature inside the magnetic and density cavities. Our objective here is to report results of a hybrid-Vlasov simulations of ion-Larmor-radius sized plasma density cavities with parameters that are representative of the high-beta solar wind plasma at the Earth's bow shock. We observe the asymmetric self-steepening and shock-formation of the cavity, and a strong localized temperature increase (by a factor of 5–7) of the plasma due to reflections and shock surfing of the ions against the collisionless shock. Temperature maxima are correlated with density minima, in agreement with Cluster observations. For oblique incidence of the solar wind, we observe efficient acceleration of ions along the magnetic field lines by the shock drift acceleration process.

Large-amplitude density and magnetic field structures have been observed in the solar wind by a number of spacecraft. The Ulysses spacecraft has observed magnetic holes characterized by a local temperature increase and increase of the plasma beta [1]. In the near-Earth solar wind, observations include hot diamagnetic cavities observed by the ISEE-1 and -2 spacecraft upstream the Earth's bow shock [2], and foreshock cavities observed by the Wind satellite [3]. In the upstream region of the Earth's bow shock, the Cluster and Double Star satellites have recently recorded density and magnetic holes with sizes of a few ion gyroradii [4]. They are associated

[1] Author to whom any correspondence should be addressed.

PII: S1367-2630(07)49118-2

with a strong heating of the plasma inside the cavities, where the temperature often rises by a factor 10 or more compared to that of the surrounding plasma. The shape of the holes are often asymmetric, representing a shock-like structure at the steepened edge facing the upstream solar wind. At the steepened edge, the plasma density and magnetic field strength can rise to several times the values of the solar wind plasma.

In this paper, we present hybrid-Vlasov simulation results which reveal interesting dynamics of a magnetic hole in the solar wind upstream the Earth's bow shock. The magnetic hole is associated with a plasma cavity, which has locally a speed smaller than that of the solar wind, so that a shock is formed on the side of the plasma cavity that faces the upwind solar wind. In our simulation, the electrons are assumed to be massless and isothermal, while the ions are treated kinetically. The inertialess electron momentum equation and Ampère's law, together with the quasineutrality condition $n_e = n_i \equiv n$, yield the electric field

$$\mathbf{E} = -\left(\mathbf{v}_i - \frac{\nabla \times \mathbf{B}}{\mu_0 e n}\right) \times \mathbf{B} - \frac{k_B T_{e0}}{e} \nabla \ln\left(\frac{n}{n_0}\right), \tag{1}$$

and the magnetic field is obtained from Faraday's law

$$\frac{\partial \mathbf{B}}{\partial t} = -\nabla \times \mathbf{E}, \tag{2}$$

where e is the magnitude of the electron charge, μ_0 is the vacuum permeability, k_B is Boltzmann's constant, T_{e0} is the unperturbed electron temperature, and n_0 is the equilibrium ion (proton) number density. The ion number density n and ion velocity $\mathbf{v}_i$ are obtained as the zeroth and first moment, respectively, of the ion distribution function. The latter is found by solving the ion Vlasov equation

$$\frac{\partial f_i}{\partial t} + \mathbf{v} \cdot \nabla f_i + \frac{e}{m_i}(\mathbf{E} + \mathbf{v} \times \mathbf{B}) \cdot \frac{\partial f_i}{\partial \mathbf{v}} = 0, \tag{3}$$

with a Fourier method [5]. While the hybrid-Vlasov code is designed for solving the ion Vlasov equation in three spatial and three velocity dimensions, plus time, we here restrict the simulation domain to one spatial dimension, along the x-direction, and three velocity dimensions, plus time.

We use parameters typical for the solar wind upstream the Earth's bow shock [4], with the ion number density $n_0 = 2.5\,\mathrm{cm}^{-3}$, the magnetic field $B_0 = 5\,\mathrm{nT}$, the ion temperature $T_{i0} = 0.5\,\mathrm{MK}$ ($1\,\mathrm{MK} = 10^6\,\mathrm{K}$), and the electron temperature $T_{e0} = 2T_{i0}$; this gives a plasma beta of $2\mu_0 n_0 k_B T_e / B_0^2 \sim 4$. The upstream side of the solar wind is assumed to be on the right-hand side of the simulation box, and the downstream side is assumed to be on the left-hand side, and the simulation box is assumed to be in the frame of the bulk plasma of the solar wind. In the centre of the simulation box, we assume a local plasma density and magnetic field hole/depletion, which is almost stationary in the frame of the Earth's bow shock, and which initially is moving in the positive x-direction against the streaming solar wind. To set the initial conditions for the simulation, we use simple-wave solutions found for nonlinear magnetosonic waves in a hot plasma [6]. In the initial conditions of the simulations, the z-component of the magnetic field is assumed to be a localized depletion of the form

$$B_z(x) = B_0\left[1 - 0.9\,\mathrm{sech}\left(\frac{x - 17\,500}{2830}\right)\right], \tag{4}$$

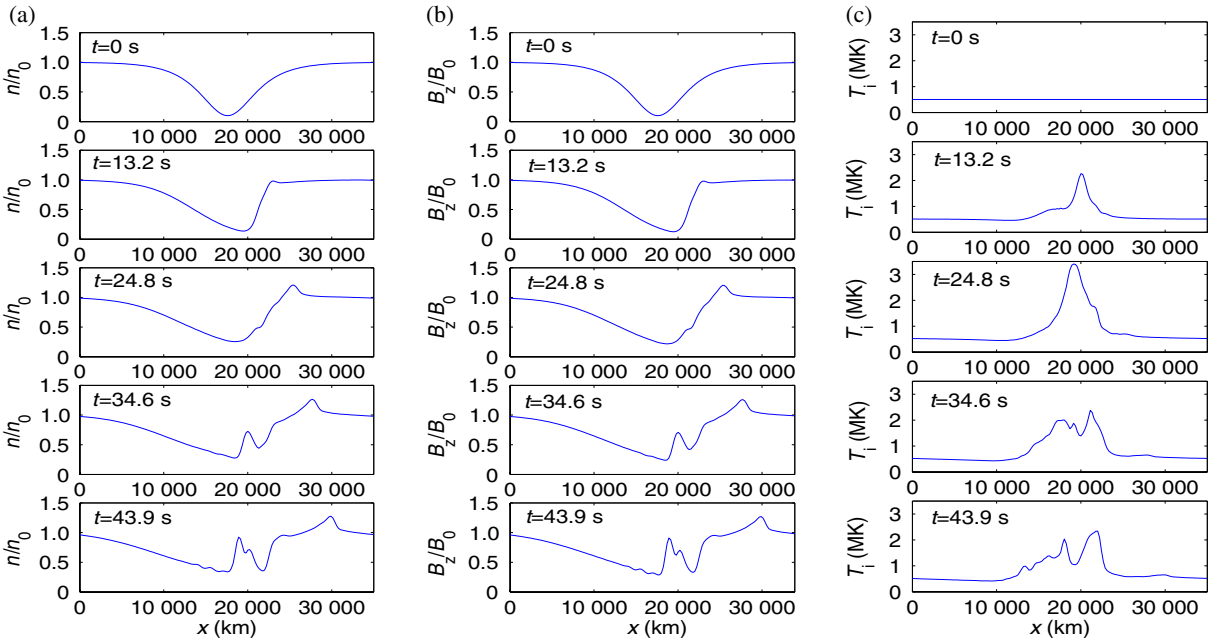

Figure 1. (a) The ion number density, (b) the magnetic field, and (c) the ion temperature at times $t = 0$, 13.2, 24.8, 34.6, and 43.9 s (top to bottom rows), for the purely perpendicular case $B_x = B_y = 0$. Here $n_0 = 2.5 \times 10^6\,\mathrm{m}^{-3}$ and $B_0 = 5\,\mathrm{nT}$.

(x in kilometres) with $B_0 = 5\,\mathrm{nT}$; see figure 1(b) at $t = 0$. The ion distribution function is taken to be

$$f_\mathrm{i}(x, \mathbf{v}) = \frac{n_\mathrm{i}(x)}{(2\pi v_{T\mathrm{i}}^2)^{3/2}} \exp\left[-\frac{(v_x - u_{\mathrm{i}x}(x))^2 + v_y^2 + v_z^2}{2v_{T\mathrm{i}}^2}\right], \tag{5}$$

where $v_{T\mathrm{i}} = (k_\mathrm{B} T_{\mathrm{i}0}/m_\mathrm{i})^{1/2} \simeq 64.3\,\mathrm{km\,s}^{-1}$ is the ion thermal speed. The ion number density is obtained from the frozen-in-field condition as $n_\mathrm{i}(x) = n_0 h(x)$ where $h(x) = B_z(x)/B_0$. From the theoretical treatment of the nonlinear magnetosonic simple-wave solutions [6], the ion mean speed along the x-direction is taken to be $u_{\mathrm{i}x}(x) = -2v_A(\sqrt{h+\beta} - \sqrt{1+\beta}) - v_A\sqrt{\beta}\ln\left[h(\sqrt{1+\beta} + \sqrt{\beta})^2/(\sqrt{h+\beta} + \sqrt{\beta})^2\right]$, where $v_A = B_0/(\mu_0 n_0 m_\mathrm{i})^{1/2} \simeq 69\,\mathrm{km\,s}^{-1}$ is the Alfvén speed and we here use $\beta = k_\mathrm{B}(T_{\mathrm{e}0} + 3T_{\mathrm{i}0})/m_\mathrm{i} v_A^2$. For the given parameters, the maximum initial mean speed of the ions along the x-direction at the centre of the density hole is $\sim$300 km s^{-1}.

In the first simulation, we assume that the magnetic field is perpendicular to the propagation (x-) direction, with $B_x = B_y = 0$, and with the z-component of the magnetic field given by equation (4) at $t = 0$. In figure 1, we have plotted the ion number density, the magnetic field and the ion temperature at different times, and in figure 2, we have visualized the corresponding ion particle distribution in (x, v_x, v_z) space. In doing so, the ion distribution function has been integrated over v_y space. The effective ion temperature has been estimated as $T_\mathrm{i} = (m_\mathrm{i}/k_\mathrm{B})(\langle \mathbf{v}^2\rangle - \langle \mathbf{v}\rangle^2)/3$ where $\langle \mathbf{v}\rangle$ and $\langle \mathbf{v}^2\rangle$ denote the first and second moment, respectively, of the ion distribution function. The initially symmetric density and magnetic field cavities, shown at $t = 0$ in panels (a) and (b), respectively, of figure 1, first propagate in the positive x direction with a speed $\sim$300 km s^{-1}, and at time $t = 13.2$ s, we see that a shock front has been formed at the right-hand flank of the plasma cavity at $x \approx 20\,000$ km. Associated with the shock front, there

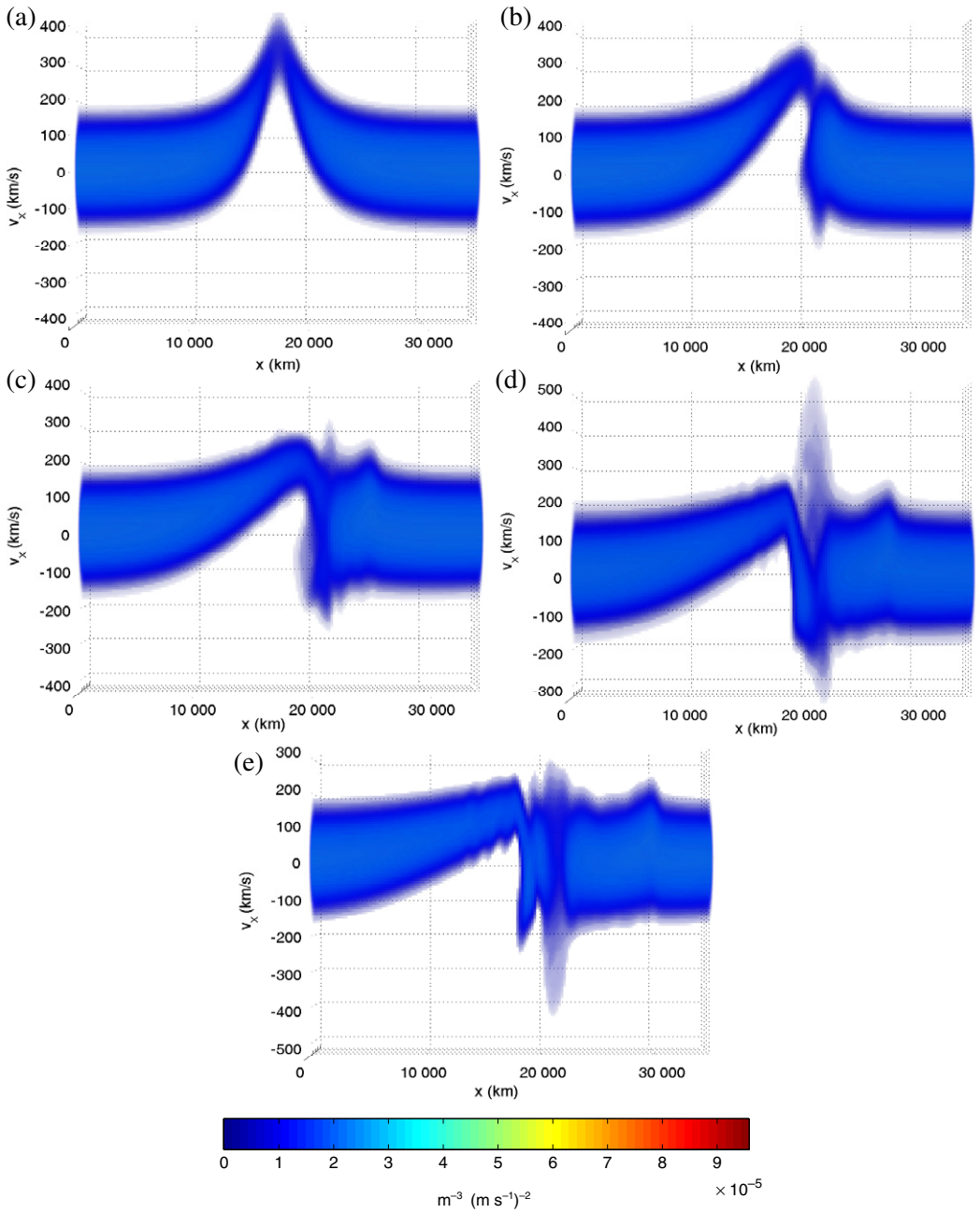

Figure 2. The ion distribution function $f_i(x, v_x, v_z, t)$ (integrated over v_y space), at times (a) $t = 0$ s, (b) $t = 13.2$ s, (c) $t = 24.8$ s, (d) $t = 34.6$ s, and (e) $t = 43.9$ s, for the purely perpendicular case $B_x = B_y = 0$.

exists a strong increase of the ion temperature, which peaks at $T_i = 3.5$ MK (i.e. seven times larger than the temperature of the solar wind) seen in (c) at $t = 24.8$ s. In the ion distribution function in figure 2, we see in panels (d) and (e) a strongly accelerated and heated population of the ions located at $x = 20\,000$–$22\,000$ km. The increase of the temperature can be explained by the fact that specularly reflected ions make the ion distribution function wider in front of the shock front and hence make the temperature larger. The temperature can be estimated as [7]

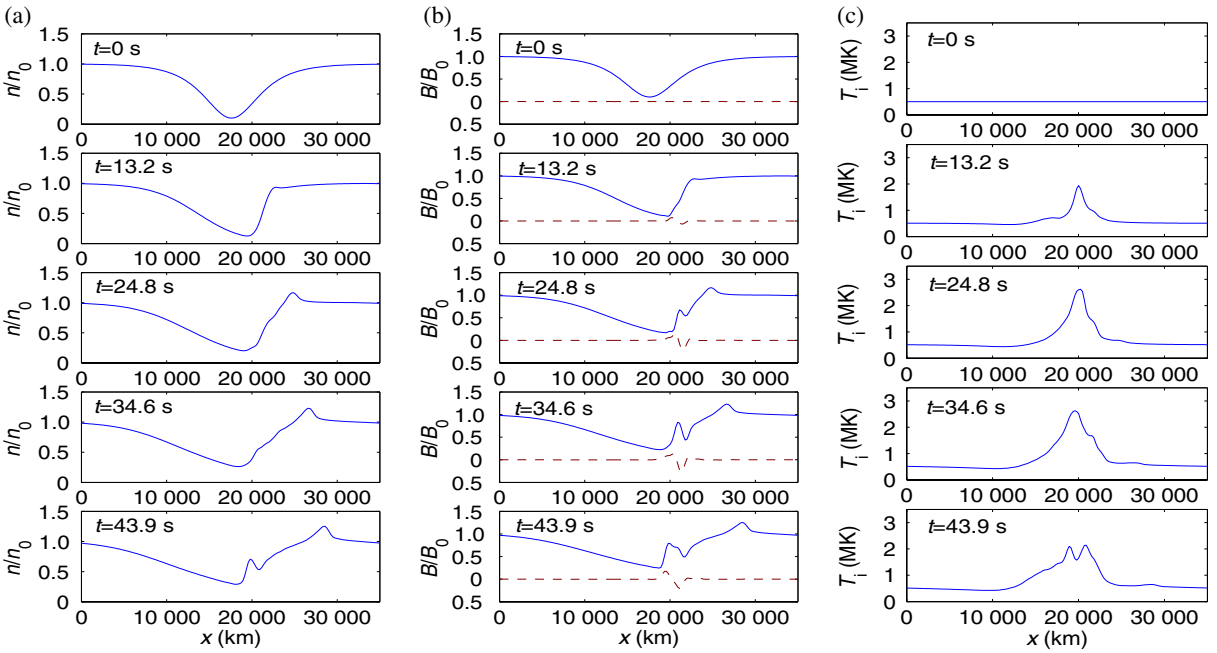

Figure 3. (a) The ion number density, (b) the magnetic field, and (c) the ion temperature at times $t = 0, 13.2, 24.8, 34.6$, and 43.9 s (top to bottom rows). Here $n_0 = 2.5 \times 10^6\,\mathrm{m}^{-3}$ and $B_0 = 5\,\mathrm{nT}$. The parallel magnetic field was $B_x = 1\,\mathrm{nT}$. In (b), the solid lines denote B_z/B_0 and the dashed lines denote B_y/B_0.

$T_\mathrm{f} \approx 4\nu_\mathrm{i}\nu_\mathrm{r}m_\mathrm{i}(v_\mathrm{in})^2/3k_\mathrm{B}$, where $\nu_\mathrm{i} = n_\mathrm{i}/(n_\mathrm{i}+n_\mathrm{r})$, $\nu_\mathrm{r} = n_\mathrm{r}/(n_\mathrm{i}+n_\mathrm{r})$, n_i (n_r) is the number density of the incident (reflected) ion population, and v_in is the speed of the incident ions relative to the shock front. In our case, with $n_\mathrm{r} = 0.5n_\mathrm{i}$, say, and $v_\mathrm{i} = 300 \times 10^5\,\mathrm{m\,s}^{-1}$, we have the temperature $T_\mathrm{f} \approx 3.5\,\mathrm{MK}$, which is the maximum temperature we observe in the simulation. We emphasize that the distribution function may be far from Maxwellian so it can be misleading to refer to T_f as a true temperature [7]. In the simulation, we also observe the development of magnetic field and density maxima which propagate to the right of the cavity with a speed of approximately $250\,\mathrm{km\,s}^{-1}$, and which is located at $x \approx 30\,000\,\mathrm{km}$ at $t = 49.3\,\mathrm{s}$. This hump is associated with a relatively small ion temperature fluctuation, which is also a feature of the much larger density and magnetic field maxima, as observed in Cluster data (cf figure 2 of [4]). At the end of the simulation at $t = 43.9\,\mathrm{s}$, we observe that maxima in the temperature is associated with minima in the density and magnetic field. This is in line with observations [4], where a 10-fold increase of the ion temperature is associated with the ion and magnetic field holes. The width of the ion temperature maximum is comparable with the ion gyroradius inside the cavity where the minimum magnetic field is of the order 0.5 nT. An ion with the speed $300\,\mathrm{km\,s}^{-1}$ would have the gyroradius 6000 km, which is of the same order as the width of the temperature maximum seen in (c) of figure 1. We note from (a) and (b) of figure 1 that the frozen-in-field condition ($n/n_0 = B_z/B_0$) is fulfilled almost completely throughout the simulation.

Next, we present the results of a different simulation with an oblique magnetic field, where B_z initially is given by equation (4), the y-component $B_y = 0$, and where the constant magnetic field along the x-direction is $B_x = 1\,\mathrm{nT}$. The ion number density, the magnetic field and the ion temperature are presented in figure 3, while the ion distribution function is depicted in figure 4. Again, the density and magnetic field cavities, shown at $t = 0$ in panels (a) and (b) in figure 3, first

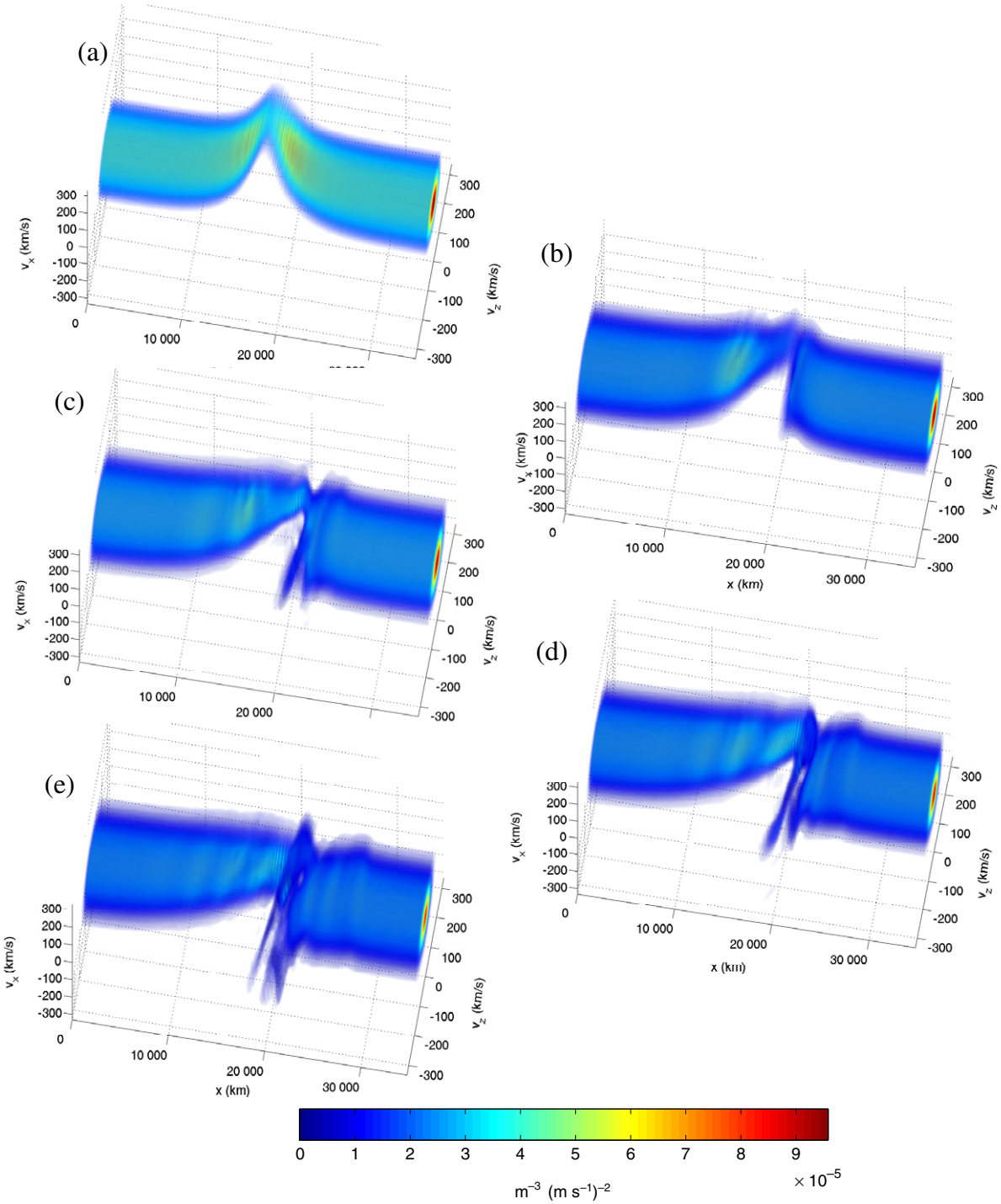

Figure 4. The ion distribution function $f_i(x, v_x, v_z, t)$ (integrated over v_y space), at times (a) $t = 0$ s, (b) $t = 13.2$ s, (c) $t = 24.8$ s, (d) $t = 34.6$ s, and (e) $t = 43.9$ s. The parallel magnetic field is set to $B_x = 1$ nT.

propagate towards the positive x-axis with a speed $\sim 300\,\mathrm{km\,s^{-1}}$, and at $t = 13.2\,\mathrm{s}$, a shock front is formed at $x \approx 20\,000\,\mathrm{km}$. Associated with the shock front, we observe a temperature increase from $T_\mathrm{i} = 0.5\,\mathrm{MK}$ to 2 MK of the ions, as seen in (c) of figure 3 at $t = 13.2\,\mathrm{s}$. Comparing (a) and (b), we see that the frozen-in-field law of the plasma is broken locally at $x \approx 21\,000\,\mathrm{km}$, where the perturbations of the magnetic field deviate from the density perturbations. Here, perturbations of B_y are also visible. In this region, we also observe an efficient acceleration of the ions along the magnetic field lines, primarily in the negative z-direction, clearly seen in panels (c)–(e) of figure 4, where the ions reach speeds of 300–400 $\mathrm{km\,s^{-1}}$. The acceleration along the magnetic field lines at quasi-perpendicular shocks can be understood in terms of shock drift acceleration [8]–[12] in which suprathermal ions, preheated by, for example, the specular reflection process [7, 8], are reflected by the shock front and drift along the magnetic field lines with a speed several times the shock speed. The acceleration of ions at the Earth's quasi-perpendicular bow shock has been observed by several spacecraft in the past, such as the Vela [13], the ISEE 1 and 2 [9], and the IMP-6, 7 and 9 [12] satellites. In general, larger magnetic fields and speeds of the solar wind lead to more efficient shock drift acceleration [12]. In our case, the ions are reflected against the shock at the right-hand side of the magnetic hole, after which they drift along the magnetic fieldlines towards the centre of the magnetic hole. The acceleration of ions is a kinetic effect, not governed by the magnetohydrodynamic model, which may explain the violation of the frozen-in law observed in figure 3. Similar to the first simulation, we also observe the development of magnetic field and density maxima propagating to the right of the cavity with a speed of approximately $250\,\mathrm{km\,s^{-1}}$, and which is located at $x \approx 30\,000\,\mathrm{km}$ at $t = 49.3\,\mathrm{s}$. At the end of the simulation, we observe in (c) of figure 3 large-amplitude temperature maxima that peak in the shock region $x \simeq 20\,000\,\mathrm{km}$.

In summary, we have investigated by a hybrid-Vlasov simulation the formation and dynamics of plasma density and magnetic holes in the upstream region of the quasi-perpendicular shock region of the solar wind. Our simulations reveal the nonlinear self-steepening and shock formation of the density hole and the local heating of the plasma due to specular reflection of the ions against the shock front. The ion temperature rises locally by a factor 5–7 times the surrounding temperature, in line with the observations where even larger temperature increases have been recorded [4]. The expansion of the locally heated plasma may result in the accelerated expansion of the density holes observed in Cluster data [4]. We expect that the heated ions can give rise to long-lived structures characterized by local density and magnetic field minima and temperature maxima, frozen into the magnetized plasma. For the oblique shock, we also observe an efficient acceleration of the ions along the magnetic field lines, owing to the shock drift acceleration [8]–[12]. There are also magnetic holes and humps observed in the heliosheath upstream of the termination shock [14, 15]. These structures have typical sizes of the order 10–20 Larmor radii of the thermal protons in the supersonic solar wind, which is larger than the holes observed by Cluster [4], which have a typical size of 3 Larmor radii. The holes observed in the heliosheath also have a more symmetric, Gaussian shape without the clear shock structure of the ones observed by Cluster; hence the magnetic holes in the heliosheath may have a different origin and dynamics than those studied here. The simulation study presented here should be helpful in understanding the dynamics of some of the density and magnetic holes that are observed in the solar wind at quasi-perpendicular bow shocks.

Acknowledgments

This work was financially supported by the Swedish Research Council. The computer resources were provided by the Swedish High Performance Computing Center North (HPC2N).

References

[1] Winterhalter D, Goldstein B E, Neugebauer M, Smith E J, Tsurutani B, Bame S and Balogh A 1995 *Space Sci. Rev.* **72** 201
[2] Thomsen M F *et al* 1986 *J. Geophys. Res. Space Phys.* **91** 2961
[3] Sibeck D G, Phan T-D, Lin R, Leppling R P and Szabo A S 2002 *J. Geophys. Res.* **107** 1271
[4] Parks G K *et al* 2006 *Phys. Plasmas* **13** 050701
[5] Eliasson B 2007 Outflow boundary conditions for the three-dimensional Vlasov-Maxwell system *J. Comput. Phys.* at press
[6] Shukla P K, Eliasson B, Marklund M and Bingham R 2004 *Phys. Plasmas* **11** 2311
[7] Sckopke N, Paschmann G, Bame S J, Gosling J T and Russel C T 1983 *J. Geophys. Res.* **88** 6121
[8] Sonnerup B U Ö 1969 *J. Geophys. Res. Space Phys.* **74** 1301
[9] Paschmann G, Sckopke N, Asbridge J R, Bame S J and Gosling J T 1980 *J. Geophys. Res.* **85** 4689
[10] Burgess D 1987 *J. Geophys. Res.* **92** 1119
[11] Giacalone J 1992 *J. Geophys. Res.* **97** 8307
[12] Anagnostopoulos G C 1994 *Phys. Scr.* **T52** 142
[13] Asbridge J R, Bame S J and Strong I B 1968 *J. Geophys. Res.* **73** 5777
[14] Burlaga L F, Ness N F and Acuna M H 2006 *Astrophys. J.* **642** 584
[15] Burlaga L F, Ness N F and Acuna M H 2006 *Geophys. Res. Lett.* **33** L21106